2016

Electron attachment to the interhalogen compounds ClF, ICl, and IBr

Justin P. Wiens
Kirtland Air Force Base

Jordan C. Sawyer
Kirtland Air Force Base

Thomas M. Miller
Kirtland Air Force Base

Nicholas S. Shuman
Kirtland Air Force Base

Albert A. Viggiano
Kirtland Air Force Base

See next page for additional authors

Authors

Justin P. Wiens, Jordan C. Sawyer, Thomas M. Miller, Nicholas S. Shuman, Albert A. Viggiano, Marjan Khamesian, Viatcheslav Kokoouline, and Ilya I. Fabrikant

Electron attachment to the interhalogen compounds ClF, ICl, and IBr

Justin P. Wiens,[1] Jordan C. Sawyer,[1] Thomas M. Miller,[1] Nicholas S. Shuman,[1] Albert A. Viggiano,[1,*] Marjan Khamesian,[2] Viatcheslav Kokoouline,[2] and Ilya I. Fabrikant[3]

[1]*Air Force Research Laboratory, Space Vehicles Directorate, Kirtland Air Force Base, New Mexico 87117, USA*
[2]*Department of Physics, University of Central Florida, Orlando, Florida 32816, USA*
[3]*Department of Physics and Astronomy, University of Nebraska, Lincoln, Nebraska 68588, USA*

Thermal electron attachment rate coefficients for three interhalogen compounds (ClF, ICl, IBr) have been measured from 300 to 900 K at pressures of 1–2 Torr using a flowing afterglow–Langmuir probe apparatus. ClF attaches somewhat inefficiently ($k = 7.5 \times 10^{-9}$ cm^3 s^{-1}) at 300 K, with the rate coefficient rising to 1.7×10^{-8} cm^3 s^{-1} at 700 K. At higher temperatures the apparent rate coefficient falls steeply; however, this is interpreted as an artifact due to decomposition on the walls of the inlet line. ICl attaches with even lower efficiency ($k = 9.5 \times 10^{-10}$ cm^3 s^{-1} at 300 K) and a less steep increase with temperature. Attachment to IBr is too slow to confidently measure with the present experiment, with an upper limit on the rate coefficient of 10^{-10} cm^3 s^{-1} from 300 to 600 K. Both ClF and ICl attach dissociatively to yield Cl$^-$, likely exclusively, though F$^-$ or I$^-$ may be produced with limits of $<2\%$ and $<5\%$, respectively. The ClF attachment was further explored through *ab initio* calculation of the ClF and ClF$^-$ potential energy curves and R-matrix calculations of the resonance parameters which were used then for calculations of the dissociative attachment cross sections and rate coefficients. While the magnitude of the attachment rate coefficient for ClF is similar to those for both Cl$_2$ and F$_2$, the calculated cross sections show qualitatively different threshold behavior due to the s-wave contribution allowed by the lack of inversion symmetry. The $v = 1$ and 2 vibrational modes of ClF attach about three to four times faster than $v = 0$ and 3 at energies lower than $\sim$0.2 eV. The calculated rate coefficients are in good agreement with the experiment at 300 K and increase moderately less steeply with temperature.

I. INTRODUCTION

The literature on low-energy electron attachment to homonuclear diatomic halogens is extensive, if at times conflicted [1–8]. These are the simplest systems that can undergo dissociative electron attachment (DEA) at thermal energies, making them attractive targets for theoretical methods aimed at handling the complexities of electron-molecule interactions. They are also obvious subjects for experiment, and measurements of the attachment kinetics to homonuclear diatomic halogens extend back to the 1920s, the earliest days of any quantitative data on electron attachment rates [9,10]. We briefly review the state of understanding of attachment to homonuclear diatomic halogens, and then address the interest in extending such studies to the interhalogen (i.e., heteronuclear diatomic halogens) species.

Experiment and theory of attachment to F$_2$ have been at odds in determining the threshold behavior as a function of energy [2,5,6]. The high-resolution experiment of Braun *et al.* for F$_2$ showed that the difficulty among experiments was that a p-wave threshold could be observed only for electron energies below 20 meV [2]. The shape of the cross sections observed by Braun *et al.* (0–180 meV electron energy) has not been reproduced by any theoretical effort thus far [2,5,6]. However, R-matrix calculations agree with thermal (300–700 K) rate coefficients for attachment to F$_2$, provided that the experimental data are used to decide between the available choices of resonance widths [5]. Likewise, a completely *ab initio* nonlocal theory gave results that agree with the thermal data [11].
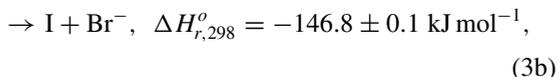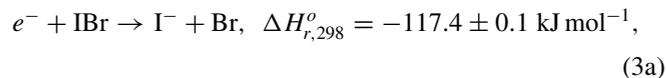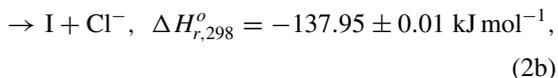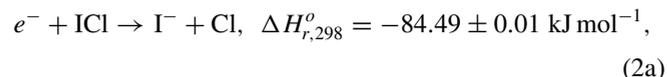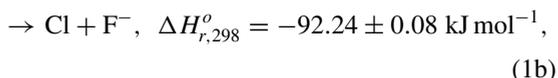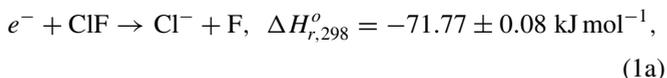
For Cl$_2$, several experiments showed a cross section for attachment that implied a peak in the cross section near zero energy, but the energy resolution precluded drawing any conclusions regarding threshold behavior [12]. R-matrix calculations demonstrated that only p-wave ($l = 1$) attachment could contribute at sufficiently low energies owing to the parity change between the $^1\Sigma_g^+$ neutral and $^2\Sigma_u^+$ anion ground states, leading to an $E^{1/2}$ behavior near threshold (i.e., a vanishing cross section at zero energy) [13]. Furthermore, the calculations showed that the Franck-Condon factor between neutral and anion drops rapidly with energy, resulting in a peak in the cross section at low energies. High-resolution experiments were carried out by Barsotti *et al.* [3] and Ruf *et al.* [7], which demonstrated p-wave behavior at meV energies along with a peak occurring at 50 meV, in agreement with theory [3,13]. Subsequent R-matrix calculations were shown as well to be in good agreement with thermal (300–1100 K) attachment rate coefficients, including high temperatures where Cl$_2$ vibrational excitation has a large effect on the attachment [8]. This agreement shows that the calculations of the vibrationally state-selected rate coefficients are probably the best example of quantum-specific values for any electron attachment system.

Older data exist for electron attachment to I$_2$ and Br$_2$ at 300 K, though the rate coefficients are not particularly well determined [1]. Minimal theoretical attempts have been made for these systems [14]. Reported rate coefficients for attachment to Br$_2$ at 300 K vary from $\sim$10^{-12} to 10^{-10} cm^3 s^{-1}. A flowing afterglow measurement for Br$_2$ yielded a value of $1.0 \pm 0.9 \times 10^{-11}$ cm^3 s^{-1} (for an electron temperature of 350 K) [15]. The few measurements for I$_2$ imply a rate coefficient $\sim$2$\times$10^{-10} cm^3 s^{-1} at 300 K [1]. Impurities complicate measurements for such small rate coefficients.

---

*afrl.rvborgmailbox@kirtland.af.mil

To our knowledge, electron attachment to the interhalogens has not been studied through experiment or theory. Several of the interhalogen diatomics are commercially available, and these are the subject of the present study. ClF, ICl, and IBr are readily available, while BrF, IF, and BrCl are not. The heats of formation of all six compounds are well established; however, the electron affinities are not. Only IBr has a clearly determined electron affinity $(2.512 \pm 0.003 \, \text{eV})$ [16], aside from a theoretical result for ClF $(2.25 \pm 0.10 \, \text{eV})$ [17]. The uncertainty in the electron affinities has little effect on the present study, as in all cases dissociative electron attachment is exothermic and there is no possibility of stabilizing the parent anion under the relatively low-pressure conditions used in the present experiments.

Unlike for attachment to the homonuclear diatomic species, for the interhalogens two product channels are energetically accessible in all cases:

$$e^- + \text{ClF} \rightarrow \text{Cl}^- + \text{F}, \quad \Delta H^o_{r,298} = -71.77 \pm 0.08 \, \text{kJ} \, \text{mol}^{-1}, \tag{1a}$$

$$\rightarrow \text{Cl} + \text{F}^-, \quad \Delta H^o_{r,298} = -92.24 \pm 0.08 \, \text{kJ} \, \text{mol}^{-1}, \tag{1b}$$

$$e^- + \text{ICl} \rightarrow \text{I}^- + \text{Cl}, \quad \Delta H^o_{r,298} = -84.49 \pm 0.01 \, \text{kJ} \, \text{mol}^{-1}, \tag{2a}$$

$$\rightarrow \text{I} + \text{Cl}^-, \quad \Delta H^o_{r,298} = -137.95 \pm 0.01 \, \text{kJ} \, \text{mol}^{-1}, \tag{2b}$$

$$e^- + \text{IBr} \rightarrow \text{I}^- + \text{Br}, \quad \Delta H^o_{r,298} = -117.4 \pm 0.1 \, \text{kJ} \, \text{mol}^{-1}, \tag{3a}$$

$$\rightarrow \text{I} + \text{Br}^-, \quad \Delta H^o_{r,298} = -146.8 \pm 0.1 \, \text{kJ} \, \text{mol}^{-1}, \tag{3b}$$

the difference in exothermicities $\Delta H^o_{r,298}$ between the channels being the difference in electron affinities of the product halides. Additionally, s-wave attachment is possible between the neutral and anion ground states. It is therefore expected that attachment to the interhalogens may be fundamentally distinct from the well-studied attachments to the homonuclear halogens.

Here we report thermal electron attachment rate coefficients from 300 to 900 K for three interhalogen diatomics, filling in a lacuna in the literature. We also apply fixed-nuclei R-matrix scattering calculations combined with the local theory of dissociative attachment [18] to one of those systems, ClF. Successful treatment regarding thermal electron attachment to ClF provides confidence to the approach made in previous attempts, including F_2, for which theory still requires refinement.

II. EXPERIMENTAL DETAILS

Attachment measurements were performed using the flowing afterglow–Langmuir probe (FALP) and high-temperature (HT-FALP) apparatuses at the Air Force Research Laboratory. The reader is referred to prior publications for further details on these instruments, with brief descriptions given here [19–22]. In the experiments, a weakly ionized plasma is created by a microwave discharge through a 10–18 standard liter min^{-1} (SLM) flow of helium (99.999%, Matheson). Ar (99.999%,

Matheson) is added at several percent of the total flow ($\sim$0.1–2 SLM) to convert He_2^+ and He^* metastables into Ar^+; the plasma at this point is $\sim$95% Ar^+/e^-, with a few percent He^+ and impurities from parts-per-million air and water impurities in the apparatus. The FALP experiments were performed at 300–600 K, and the HT-FALP was operated from 300 to 900 K. Temperatures were controlled by resistive heating elements positioned along the flow tube length, with temperature sensors positioned on the flow tube walls. In both setups a preheated zone was set $\sim$10%$-$20% higher than the desired measurement temperature, in order to achieve a flat temperature gradient along the reaction zone. Calibration of the sensors was previously verified by translating a thermocouple along the flow tube axis to monitor the buffer gas temperature. All gas flows were metered with mass flow controllers (MKS Instruments). Pressures of 1–2 Torr [$(3-6) \times 10^{16}$ molecules cm^{-3} at 300 K] were used in the experiments.

Reactant gases were added approximately halfway down the flow tube through a glass (FALP) or quartz (HT-FALP) inlet with multiple equally spaced hollow needles pointing radially into the flow tube to achieve better gas distribution into the flowing He-Ar buffer. The gas feed line to the inlet is different in the two apparatuses. In the FALP, a glass tube runs 50 cm from the *downstream* end of the flow tube to the inlet. In the HT-FALP, a quartz tube runs from the *upstream* end to the inlet, which means that the reactant must first pass through the preheated zone. This latter method may cause thermal decomposition of reactant gas at temperatures lower than the nominal temperature in the reaction zone.

Absolute electron densities were monitored with a cylindrical Langmuir probe composed of tungsten wire (FALP, 7.7 mm $\times$ 0.025 mm diam; HT-FALP, 7.8 mm $\times$ 0.076 mm diam) centered on the flow tube axis. In each apparatus the probe could be translated along the axis of the flow tube (FALP, 15 cm upstream to 35 cm downstream of the reactant inlet; HT-FALP, 1–26 cm downstream of the inlet) to determine electron losses due to attachment to the reactant, or diffusion in the absence of added reactant. A sample data run is shown in Fig. 1. The time scale for the measurements comes from measurements of the plasma velocity. Plasma velocities of 50–180 m/s were routinely determined in the FALP using a pulsed disturbance to the microwave discharge and noting the arrival time of the disturbance at the Langmuir probe as it was translated along the flow tube. In the HT-FALP a series of such measurements was carried out. The plasma velocity for each data run was then calculated from the measured ratio of the plasma velocity to the bulk velocity of the buffer gas.

Ions were sampled through a pinhole aperture followed by ion optics and a mass spectrometer. Accurate relative ion signals were not important in the experiments because the rate coefficient measurements only depend on the depletion of electrons (attachment experiments) or Ar^+ (ion-molecule experiments) and in all cases only one main product anion was observed. The spectra nevertheless provided information on impurities and progress of the passivation process, as described below.

ClF (99%) was obtained from Synquest Laboratories, Inc., as a gas and then diluted in He (99.999%, Matheson) to between 1% and 2%. IBr was obtained as dark blue crystals from Alfa Aesar and degassed by freeze-pump-thaw cycles
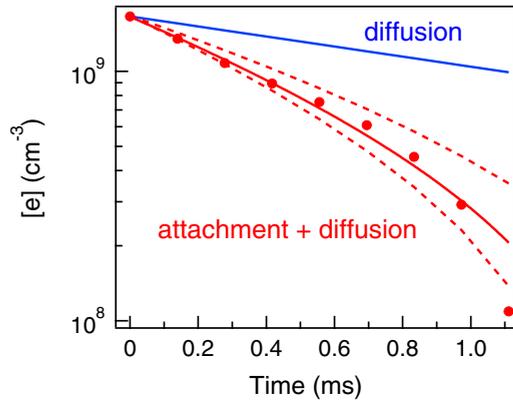
FIG. 1. Typical attachment data, shown for ICl on the FALP at 400 K. The flow tube pressure was 1.5 Torr, corresponding to a plasma velocity of 7200 cm/s, with an added ICl concentration of 8.6×10^{10} cm^{-3}. The falloff after 1.00 ms indicates collapse of the ambipolar field, resulting in sudden diffusive loss of remaining free electrons, which is not modeled. The lower solid curve (red online) represents the best fit to the attachment data (excluding the last point at 1.10 ms) with the measured ambipolar diffusion rate of 464 s^{-1} (upper solid line, blue online) included. Dashed lines represent typical $\pm 25\%$ uncertainty in the attachment rate coefficient.

in a glass flask. A steady flow of He, F_{He}, was directed into the flask that was also attached to the reactant inlet and a thermocouple pressure gauge to monitor the local pressure P_{cell}. In this arrangement, the actual flow of IBr entering the inlet F_{IBr} can be expressed as [22]

$$F_{IBr} = [(P_{vap}/P_{cell} - P_{vap})]F_{He}, \qquad (4)$$

where P_{vap} is the IBr vapor pressure at 300 K of $\sim$2 Torr. Achieving steady reactant flows of sufficiently high IBr concentration was difficult because IBr attaches electrons slowly. Limited measurements were made to provide upper bounds on the attachment rate coefficient. We suspected that IBr begins to dissociate at temperatures above $\sim$600 K, and the experiments were therefore not attempted on the HT-FALP.

ICl was obtained from Alfa Aesar as a dark, reddish brown liquid. The reagent was drawn by pipette into a glass flask and degassed by several freeze-pump-thaw cycles. ICl has two polymorphs with melting points separated by only 13 °C. The solid, β form with its vapor pressure of a couple of Torr could be obtained by warming up the frozen, degassed flask to room temperature. In order to reobtain the more stable and volatile α polymorph, the liquid form, the flask was then warmed gently. The reagent storage container and mixture manifold were maintained several degrees above room temperature when diluting the reagent to $\sim$1%–2% in He. The storage container was first evacuated and then passivated with the reagent. Over the course of the experiments, we assumed that the ICl fraction in the mixture remained the same as when the mixture was made. Due to the 14 °C melting point of the less stable β polymorph, it is unlikely that the sample reconverted to the solid in the storage container under ambient conditions. The fact that the attachment measurements were consistent over the course of several weeks is support for this assertion. A separate sample was prepared and brought to room temperature as the β form. Over the course of several hours, the sample

slowly reconverted to the α polymorph without intentional heating above room temperature, verifying that reconversion to the solid does not occur and that our nominal added ICl concentrations were consistent throughout the experiments.

Sufficient passivation of the inlet lines with the reactant was necessary to achieve consistent and reliable results from day to day. For both ICl and ClF, several standard cm^3 min^{-1} (sccm) of reactant were flowed for at least 20 min before measurements were taken, then at regular intervals until the electron depletion at a given distance and reactant flow remained constant. Neglecting this passivation would give erroneously low attachment results. For ICl measurements, Cl$^-$ was the dominant anion present in the mass spectrum, with $\lesssim$5% I$^-$ and <2% O$^-$ impurities. We measured the rate coefficient for Cl$^-$ + ICl $\rightarrow$ I$^-$ + Cl$_2$ to be <2$\times$10^{-10} cm^3 s^{-1}, by adding CCl$_4$ upstream of the reactant inlet to provide the precursor Cl$^-$; some or all of the I$^-$ may come from this channel. We obtained a similar upper bound for the analogous I$^-$ reaction forming Cl$^-$. More accurate rate coefficients for this reaction, obtained with a selected-ion flow tube apparatus, and others involving I$^-$ and Br$^-$ precursor ions and the neutrals ClF and ICl will be reported in a later publication [23]. For ClF, Cl$^-$ is formed exclusively from the attachment reaction, although OCl$^-$ and Cl$_2^-$ impurities were always present at a few percent of the total signal. These impurity signals decreased after passivation but could not be completely eliminated and are likely due to O$_2$ in the He-Ar buffer forming O$^-$, which then reacts with ClF or products of other ion processes in the plasma. For IBr measurements, the FALP was baked for at least 1 day (following ClF or ICl measurements) at 500 K, and IBr was flowed until no residual Cl$^-$ impurities were present in the anion spectrum.

Once the lines were sufficiently passivated, the attachment measurements were taken under similar flow conditions (a few sccm of reactant, $\sim$10^{10}–10^{11} cm^{-3}) at a plasma density of $\sim$10^9 cm^{-3}. These conditions were chosen such that attachment is pseudo first order in the reactant species and to ensure that ion-electron recombination has a minimal (<10%) effect on the measurements [21]. The Langmuir probe was cleaned regularly between measurements by applying several hundred volts (drawing a few mA of electrons to the probe) for 1–2 s. In the HT-FALP, this cleaning was necessary to ensure consistent probe readings at a given probe position along the flow tube axis.

Reaction of Ar$^+$ with the interhalogens was studied by monitoring the Ar$^+$ depletion as a function of added reactant concentration (10^{10}–10^{12} cm^{-3}) under pseudo-first-order conditions. In the HT-FALP, the fast-attaching gas CCl$_4$ was added in low concentrations ($\sim$10^9 cm^{-3}) to eliminate free electrons quickly so that the ambipolar diffusion rate was constant along the flow tube. Except for IBr, the rate coefficients with Ar$^+$ had nearly flat temperature dependences on both FALP instruments. The same results were observed on a selected-ion flow tube (SIFT) apparatus incorporating a stainless steel reactant gas inlet; those data will be reported separately [23].

III. THEORETICAL METHODS AND RESULTS

In the present study we use a fully *ab initio* theoretical approach based on potential energy curves of the ClF and ClF$^-$

molecules and reactance matrix $K(R)$ for e^--ClF collisions. There are several previous ClF and ClF$^-$ structure calculations based on different quantum chemistry methods: configuration interaction (CI), coupled cluster (CC) methods, and density functional theory [17,24–30]. The most accurate ClF and ClF$^-$ structure calculations have been made by Alekseev *et al.* [26] and more recently by Li *et al.* [27], who employed CI and CC methods. In Ref. [26] relativistic effects have also been accounted for. We briefly discuss below technical details of our calculations.

For structure calculations of potential energy curves of ClF and ClF$^-$, the MOLPRO suite [31] has been employed. In DEA theory, accurate determination of crossing point(s) between potential curves of the neutral molecule and the anion is crucial. For *ab initio* calculations it means that relative energy of the neutral and anion curves should be determined as accurately as possible. With this goal, the following procedure has been tested and chosen in the present *ab initio* calculations. We use relatively large standard atomic basis sets augmented with diffuse functions with s, p, d, and f orbitals, d-aug-cc-pVQZ for fluorine and aug-cc-pVQZ for chlorine. Diffuse functions are necessary to accurately calculate anion electronic states. With this basis, Hartree-Fock orbitals have been determined for the neutral molecule. The same Hartree-Fock orbitals have been used in the second step of the calculations for the neutral and anion molecule. In that second step, natural orbitals have been determined for both molecules. To ensure accurate relative energy of the ClF and ClF$^-$ curves, not only the same Hartree-Fock orbitals, but also the same orbital space has been used in both the ClF and ClF$^-$ calculations. In practice, a much larger—compared to a standard single-molecule calculation—was needed to obtain converged results for ClF$^-$. In a typical calculation, out of 22 occupied orbitals in all symmetries, the eight lowest orbitals were kept frozen. For the neutral molecule, only the lowest $^1\Sigma^+$ electronic state has been determined. For the anion, the $^2\Sigma^+$ and the $^2\Pi$ states have been calculated. Using the natural orbitals, configuration interaction calculations have been performed as the third step for the ground $^1\Sigma^+$ electronic state of ClF and for the two lowest states for each of the $^2\Sigma^+$ and $^2\Pi$ symmetries of ClF$^-$. Again, the same orbital space for ClF and ClF$^-$ has been used.

Results of the structure calculations are shown in Fig. 2. On the right side of the graph, labels "Cl + F," "Cl + F$^-$," and "Cl$^-$ + F" with short horizontal lines refer to the Cl + F, Cl + F$^-$, and Cl$^-$ + F dissociation limits obtained in this study. The energies marked with the horizontal lines are those obtained at $R = 7$ bohrs, the largest distance where the convergence is still reasonable with the employed orbital space. The energy differences $[\text{Cl} + \text{F}] - [\text{Cl} + \text{F}^-]$ and $[\text{Cl} + \text{F}] - [\text{F} + \text{Cl}^-]$ correspond to electron affinities of Cl and F. In the present calculations $[\text{Cl} + \text{F}] - [\text{Cl} + \text{F}^-] = 3.0\,\text{eV}$ and $[\text{Cl} + \text{F}] - [\text{F} + \text{Cl}^-] = 3.4\,\text{eV}$, whereas accurate affinities of F and Cl are 3.399 and 3.617 eV, respectively. Although the difference is significant, it does not affect the DEA calculations in the crossing region where accurate curves are necessary.

Table I compares equilibrium positions R_e for ClF and ClF$^-$ obtained in the present work with several previous calculations [24–28] and an experimental work [29]. The values of R_e obtained in this study agree well with the most accurate
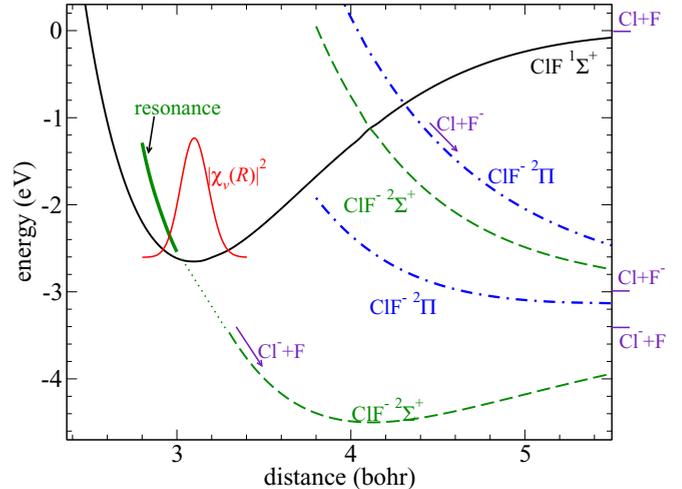

FIG. 2. Potential energy curves of ClF and ClF$^-$ molecules. The solid curve is the ground electronic state of the ClF molecule. The two lowest electronic states of the $^2\Sigma^+$ and $^2\Pi$ symmetries of ClF$^-$ are shown by dashed (green online) and dot-dashed curves (blue online), respectively. The curve labeled $|\chi_v(R)|^2$ (red online) shows the probability density of the ground vibrational level of the ClF molecule. The thick line (green online) labeled "resonance" represents the energy of the lowest resonant state of ClF$^-$. The labels "Cl + F," "Cl + F$^-$," and "Cl$^-$ + F" with short horizontal lines refer to corresponding dissociation limits as calculated in this study.

previous theoretical work by Li *et al.* [27] and with the RKR data available from the experiment [29].

Each of the lowest curves of the $^2\Sigma^+$ and $^2\Pi$ states dissociates only towards the F + Cl$^-$ limit. Out of all the ClF$^-$ curves, only the lowest $^2\Sigma^+$ state crosses the neutral state near the minimum of the ClF potential. In addition, the ground state does not approach any other curve to the right of the crossing. This suggests that if the ClF molecule is initially in one of the lowest vibrational levels, the DEA products could only be F + Cl$^-$, consistent with the experimental results presented here. Figure 2 also shows the probability density $|\chi_v(R)|^2$ of the ground vibrational level in the ClF potential, representing the Franck-Condon factor for this state. Electron beam experiments are expected to show peaks corresponding to the higher-energy ClF$^-$ states shown in Fig. 2, but these are not relevant to the present studies and would have to be calculated more accurately.

TABLE I. Equilibrium distances R_e of the ground electronic states of ClF and ClF$^-$ obtained in the present and previous studies. The most accurate theoretical calculations are from Refs. [26,27].

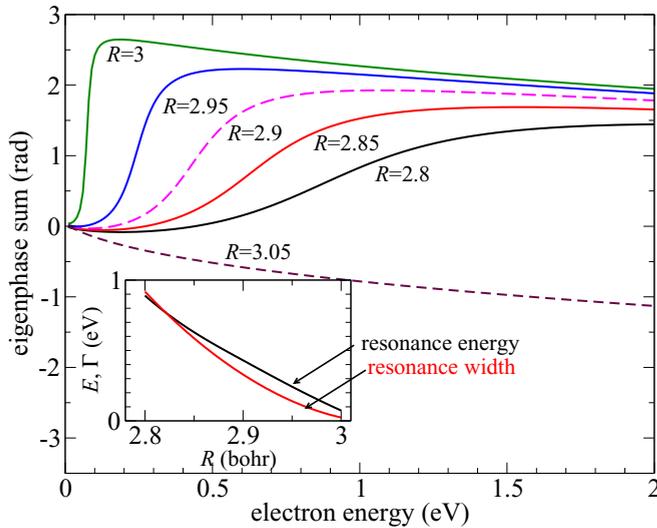|	R_e (ClF) (Å)	R_e (ClF$^-$) (Å)
Present calculations	1.638	2.181
Calc., Ref. [24]	1.614–1.668	2.049–3.036
Calc., Ref. [25]	1.643–1.659	2.078–2.298
Calc., Ref. [26]	1.641	
Calc., Ref. [27]	1.6294	2.148–2.156
Calc., Ref. [28]	1.63–1.69	2.25–2.40
Expt., Ref. [29]	1.628	

FIG. 3. The eigenphase sums for $e^- + ClF$ scattering in the $^2\Sigma^+$ symmetry for six different values of the internuclear distance R near the crossing point of the ClF and ClF$^-$ potential curves. For all shown values of R, the ClF$^-$ state is resonant, except for $R = 3.05$ bohrs, for which the ClF$^-$ electronic state is bound. The inset shows energies and widths of the resonant state. Energy E is the electron scattering energy.

The electron scattering calculations have been performed using the UK R-matrix/QUANTEMOL code [32–34]. In the calculation, the cc-pVTZ atomic basis with $l = 0-4$ orbitals have been employed for the two atoms. The target ClF molecule of the $^1\Sigma^+$ symmetry was represented using a complete-active-space configuration interaction (CASCI) method built on Hartree-Fock orbitals. The eight lowest Hartree-Fock orbitals of the target ClF have been frozen in the CASCI calculations. The remaining ten (out of 26) electrons have been distributed over the active space that included nine orbitals and six virtual orbitals. The virtual orbitals have been included in the calculations to improve the electronic continuum states near the target nuclei. ClF is a small molecule and a small R-matrix sphere radius of 10 bohrs was used.

The K matrix $K(R)$ obtained in the scattering calculations was used to determine energies and widths of the $^2\Sigma^+$ resonance for distances $R < 3.05$ bohrs, where the curve is resonant. The energies and widths were obtained from eigenphase sums generated by $K(R)$. The eigenphase sums for six values of R are shown in Fig. 3. As evident from Fig. 2, the $^2\Sigma^+$ curve of ClF$^-$ crosses the ClF $^1\Sigma^+$ potential near $R_c = 3.02$ bohrs. The inset in Fig. 3 shows the resonance energy E and width Γ as a function of R. The full resonance width is obtained from fitting the eigenphase sums to the Breit-Wigner formula [35].

Figure 2 also shows the resonance energy with the thick green line, but now the energy of the ClF $^1\Sigma^+$ potential is added to the scattering energy E. Represented in this way the resonant curve (thick green line in Fig. 2) should join smoothly the lowest $^2\Sigma^+$ curve of ClF$^-$ obtained in bound-state calculations. However, our basis in the bound-state calculations was not optimized for weakly bound states of the $^2\Sigma^+$ curve of ClF$^-$. Therefore, a part of the $^2\Sigma^+$ curve below

the crossing point is not computationally converged and is missing in Fig. 2. This part of the $^2\Sigma^+$ curve is replaced by a straight dotted line to guide the eye.

Bound-state and scattering calculations show that the anion curve is crossing the neutral close to the equilibrium internuclear separation in ClF. Although in this regard the situation is similar to that for attachment to the F$_2$ and Cl$_2$ molecules, in the case of ClF the inversion symmetry is broken, and the s-wave component in the electron wave function contributes to the resonance composition. Our calculated scattering matrices indicate a substantial intermixture of the s, p, and d waves. As an example, for internuclear distance $R = 3$ bohrs and near-resonant energy of 0.07 eV (see Fig. 3), the probability of a partial-wave change after one collision from the $s\sigma$ partial wave to $p\sigma$ is 0.49. The probabilities of the $s\sigma \to d\sigma$ and $p\sigma \to d\sigma$ transitions at the same energy and internuclear distance are significantly smaller, 0.003 and 0.01, correspondingly.

Ab initio calculation of partial attachment amplitudes presents a big challenge for the nonlocal complex potential theory [36] where the amplitudes should be calculated as functions of electron energies. But even in the local theory calculation of partial resonance widths is a nontrivial task, and, to the best of our knowledge, has been accomplished only in calculations of DEA to water [37] whose purpose was to extract information on the angular distribution of the DEA products. In the case where we are not interested in the angular distribution, we can introduce an angular-independent attachment amplitude $V(R)$ calculated as

$$V(R) = [\Gamma(R)/2\pi]^{1/2}. \qquad (5)$$

This is a common approach used in many local DEA calculations which we also use in the present paper.

After $\Gamma(R)$ and the attachment amplitude $V(R)$ are obtained, we solve the inhomogeneous equation of the local complex potential model [18] (also called the boomerang model [38]) for the wave function $\psi(R)$ describing the nuclear motion in the anion state

$$[T + U(R) - i\Gamma(R)/2 - E]\psi(R) = -V(R)\chi_v(R), \qquad (6)$$

where T is the kinetic energy operator, $U(R)$ is the anion potential energy, E is the electron energy, and $\chi_v(R)$ is the vibrational function of the molecule in the initial state.

The major deficiency of the local approximation appears in producing the DEA cross sections with incorrect threshold behavior. This is, for example, a serious issue in attachment to F$_2$ and Cl$_2$ molecules [39,40]. Due to the $^2\Sigma_u^+$ symmetry of the low-energy resonance in this case, the Wigner threshold law predicts $E^{1/2}$ energy dependence [2,13] whereas in local calculations the cross section diverges towards $E = 0$ as E^{-1}. Bardsley [41] suggested a correction for the attachment amplitude in the form of the factor

$$[E/E_r(R)]^{a/2}, \qquad (7)$$

where $E_r(R)$ is the resonance energy, that is, $U(R) - U_0(R)$, where $U_0(R)$ is the potential energy of the neutral molecule, and a is the threshold exponent. For nonpolar molecules, according to the Wigner law, $a = l + \frac{1}{2}$ where l is the lowest angular momentum allowed by symmetry. For polar molecules, depending on the dipole moment, a varies between
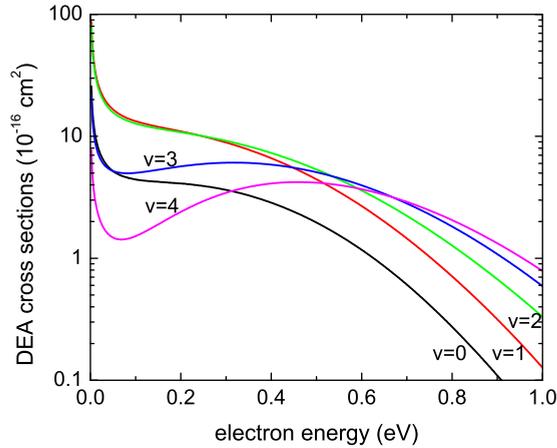
FIG. 4. DEA cross sections, calculated with Bardsley's correction, from the first five vibrational states of the ClF.

0 and $\frac{1}{2}$ [42]. In particular for the ClF molecule whose dipole moment is 0.346 a.u. (0.8881 D) [43], $a = 0.4152$. The cross section for an exothermic reaction behaves as E^{a-1} that in the case of ClF leads to $E^{-0.5848}$ behavior at low energies, in contrast to the $1/E$ behavior in the original version of the nonlocal theory. This difference is important for thermal energies.

In Fig. 4 we present the attachment cross sections for different initial vibrational states. At low electron energies the attachment cross section is largest for $v = 1$ and 2; about three to four times those for $v = 0$ and 3 at low energy. The vibrational quantum for ClF is 97.1 meV. Therefore, accounting for the Boltzmann factor, the $v = 3$ contribution is insignificant at $T = 700$ K. This dependence of the DEA cross section on v is relatively weak; that is typical for the situation when the neutral and anion curves cross close to the equilibrium internuclear separation. This results in a weak dependence of the cross section on the vibrational temperature, as demonstrated in Fig. 5.
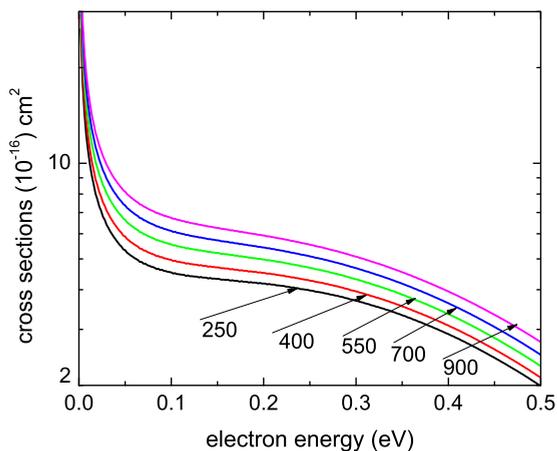

FIG. 5. DEA cross sections for ClF averaged over the vibrational-state distribution. Numbers associated with each curve indicate the vibrational temperature in degrees K.
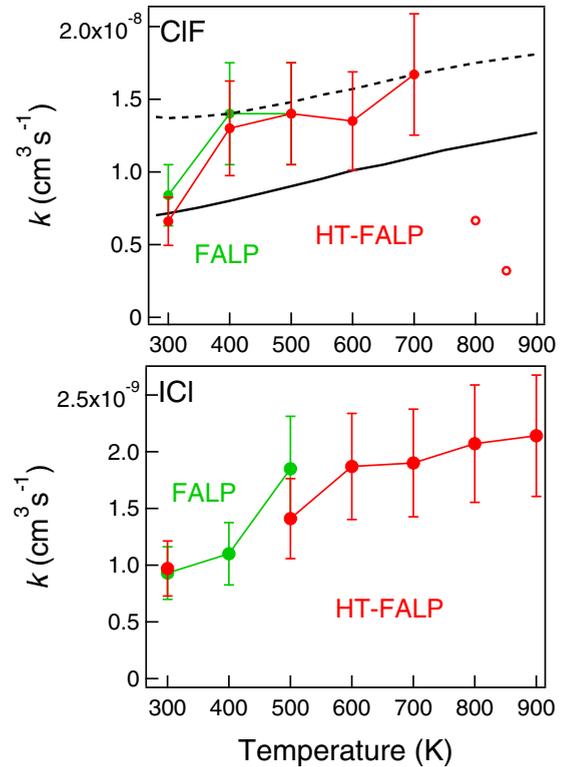

FIG. 6. Top: experimental DEA rate coefficients k (in units of cm^3 s^{-1}) for ClF from 300 to 850 K. Points connected by line segments are from the FALP apparatus (green online) and from the HT-FALP apparatus (red online). Two open symbols represent the apparent rate coefficient which may be low due to decomposition or other losses in the flow tube. The rate coefficient from electron scattering calculations is shown with (black solid line) and without (black dashed line) Bardsley's correction, as described in the text. Bottom: experimental DEA results for ICl from 300 to 900 K. Error bars in both panels are ±25%.

IV. EXPERIMENTAL RESULTS AND COMPARISON WITH THEORY

The theoretical calculations described above confirm the exclusive production of Cl$^-$ from ClF. The theoretical rate coefficients were obtained by averaging the cross sections from Fig. 5 over the electron energy distribution. The results do not show a significant temperature dependence because the low-energy behavior of the cross section is close to $E^{-1/2}$ meaning that the rate coefficient weakly depends on E. The growth of the ClF rate coefficient with temperature is slow and does not indicate any activation energy typical for Arrhenius-type behavior [44]. In Fig. 6 we show good agreement of experimental data with the second calculation at $T = 300$ K. However, the rate coefficients calculated with Bardsley's correction [41] grow slower than the experimental values. It is not unusual for Bardsley's correction to underestimate the DEA cross section; therefore it is not surprising that at $T = 700$ K the experimental result lies closer to the first calculation. Overall, considering all approximations involved in the theory, the agreement is satisfactory.

The electron attachment results for ClF, ICl, and IBr are presented in Table II and Fig. 6. The rate coefficients for ClF

TABLE II. Attachment rate coefficients k (in units of cm^3 s^{-1}) for the three interhalogens from 300 to 900 K. FALP and HT-FALP values have been averaged for data taken at the same temperatures on both instruments. Error bars for the measurements are approximately $\pm 25\%$.

	Temperature (K)						
Species	300	400	500	600	700	800	900
ClF	7.5×10^{-9}	1.4×10^{-8}	1.4×10^{-8}	1.4×10^{-8}	1.7×10^{-8}		
ICl	9.5×10^{-10}	1.1×10^{-9}	1.6×10^{-9}	1.9×10^{-9}	1.9×10^{-9}	2.1×10^{-9}	2.1×10^{-9}
IBr	$<10^{-10}$	$<10^{-10}$	$<10^{-10}$	$<10^{-10}$			

and ICl have modest, positive temperature dependences with good agreement between the FALP and HT-FALP instruments where they overlap at lower temperatures. The apparent rate coefficient for attachment to ClF falls off steeply above 700 K. Such a steep drop cannot be physical, and is typical of high-temperature decomposition of the reactant on walls of the quartz inlet line which (as discussed above) is overheated by 10%−20% in the upstream region. The rate coefficients for the ion-molecule reactions Ar$^+$ + ClF and ICl have nearly flat temperature dependences throughout the entire temperature range, rather than a falloff at high temperature. We do not know the identity of the presumed decomposition products at high temperatures. IBr attaches at $<10^{-10}$ cm^3 s^{-1} even up to 600 K. The rate coefficient for reaction with Ar$^+$ decreased from 5×10^{-10} cm^3 s^{-1} at 300 K to $\sim 2 \times 10^{-10}$ cm^3 s^{-1} at 600 K indicating that high-temperature dissociation may also be occurring.

The measured rate coefficients for Ar$^+$ + ClF and IBr, to be reported in a later publication, are approximately half of the calculated collisional value [43,45,46] from 300 to 800 K. These results are consistent with data for Ar$^+$ reacting with F$_2$ [5], Cl$_2$ [47], and Br$_2$ [47]. The implication is that passivation of the reactant gas feed lines was complete, within the uncertainties inherent to this comparison.

Both ClF and ICl dissociatively attach exclusively forming Cl$^-$, forming little or no F$^-$ or I$^-$, respectively, throughout the entire temperature range. The Cl$^-$ channel is more exothermic than forming F$^-$ from ClF by only 0.21 eV (the difference in the electron affinities of Cl and F), and from ICl by 0.55 eV; see Eqs. (1) and (2). The theoretical calculations described above imply exclusive production of Cl$^-$ from ClF. IBr attachment appears to yield both I$^-$ and Br$^-$ in the mass spectrum, but the large reactant flows required for the measurements of a slow attachment reaction mean that the (near-thermoneutral)

secondary reactions Br$^-$(I$^-$) + IBr $\rightarrow$ I$^-$ + Br$_2$(or Br$^-$ + I$_2$) complicate the analysis of product distribution.

V. CONCLUSIONS

Electron attachment to the interhalogen diatomics ClF, ICl, and IBr was studied over the temperature range 300–900 K using two flowing afterglow–Langmuir probe apparatuses. Both ClF and ICl exhibit modestly increasing rate coefficients with increasing temperature, predominantly forming Cl$^-$. The ClF trend may be slightly steeper than that predicted from theoretical calculations, but the calculated rate coefficients are nevertheless in agreement with experiment. No activation barrier to attachment is indicated by the modest trends with temperature. Similar to symmetric halogen diatomics such as Cl$_2$ and F$_2$, dissociative electron attachment to ClF occurs near the equilibrium Cl-F atomic separation. Unlike Cl$_2$ and F$_2$, the lack of inversion symmetry in ClF allows a substantial contribution of the s-wave component of the electron wave function to the scattering cross section. Theory shows that the $v = 1$ and 2 vibrational levels of ClF dominate the attachment resonance with little contribution from higher modes or $v = 0$.

[1] *Electron-Molecule Interactions and Their Applications*, edited by L. G. Christophorou (Academic Press, New York, 1984), Vols. 1 and 2.

[2] M. Braun, M.-W. Ruf, I. I. Fabrikant, and H. Hotop, Phys. Rev. Lett. **99**, 253202 (2007).

[3] S. Barsotti, M.-W. Ruf, and H. Hotop, Phys. Rev. Lett. **89**, 083201 (2002).

[4] H. Hotop, M.-W. Ruf, M. Allan, and I. I. Fabrikant, Adv. At. Mol. Opt. Phys. **49**, 85 (2003).

[5] N. S. Shuman, T. M. Miller, A. A. Viggiano, and I. I. Fabrikant, Phys. Rev. A **88**, 062708 (2013).

[6] I. I. Fabrikant, J. Phys.: Conf. Ser. **204**, 012004 (2010).

[7] M.-W. Ruf, S. Barsotti, M. Braun, H. Hotop, and I. I. Fabrikant, J. Phys. B **37**, 41 (2004).

[8] J. F. Friedman, T. M. Miller, L. C. Schaffer, A. A. Viggiano, and I. I. Fabrikant, Phys. Rev. A **79**, 032707 (2009).

[9] H. B. Wahlin, Phys. Rev. **19**, 173 (1922).

[10] N. E. Bradbury, J. Chem. Phys. **2**, 827 (1934).

[11] A. U. Hazi, A. E. Orel, and T. N. Rescigno, Phys. Rev. Lett. **46**, 918 (1981).

[12] R. J. Gulley, T. A. Field, W. A. Stevens, N. J. Mason, S. L. Lunt, J.-P. Ziesel, and D. Field, J. Phys. B **31**, 2971 (1998), and references therein.

[13] I. I. Fabrikant, T. Leininger, and F. X. Gadéa, J. Phys. B **33**, 4575 (2000).

[14] D. T. Birtwistle and A. Modinos, J. Phys. B **11**2949 (1978).

[15] G. D. Sides, T. O. Tiernan, and R. J. Hanrahan, J. Chem. Phys. **65**, 1966 (1976).

[16] L. Sheps, E. M. Miller, and W. C. Lineberger, J. Chem. Phys. **131**, 064304 (2009).

[17] . Horný, K. W. Sattelmeyer, and H. L. Schaefer, J. Chem. Phys. **119**, 11615 (2003).

[18] T. F. O'Malley, Phys. Rev. **150**, 14 (1966).

[19] N. S. Shuman, T. M. Miller, A. A. Viggiano, and J. Troe, Adv. At. Mol. Opt. Phys. **61**, 209 (2012).

[20] T. M. Miller, J. F. Friedman, J. S. Williamson, L. C. Schaffer, and A. A. Viggiano, Rev. Sci. Instrum. **80**, 034104 (2009).

[21] T. M. Miller, Adv. At. Mol. Opt. Phys. **51**, 299 (2005).

[22] A. J. Midey, S. Williams, S. T. Arnold, I. Dotan, R. A. Morris, and A. A Viggiano, Int. J. Mass Spectrom. **195**, 327 (2000).

[23] O. Martinez, S. G. Ard, J. P. Wiens, J. C. Sawyer, N. S. Shuman, and A. A. Viggiano (unpublished).

[24] M. T. Nguyen and T.-K. Ha, Chem. Phys. Lett. **136**, 413 (1987).

[25] C.-K. Law, S.-H. Chien, and W.-K. Li, J. Phys. Chem. A **106**, 11271 (2002).

[26] A. B. Alekseyev, H.-P. Liebermann, R. J. Buenker, and D. B. Kokh, J. Chem. Phys. **112**, 2274 (2000).

[27] S. Li, S.-J. Chen, D.-S. Zhu, and J.-J. Wei, Acta Phys. - Chim. Sin. **29**, 737 (2013).

[28] T. J. Van Huis, J. M. Galbraith, and H. F. Schaefer, Mol. Phys. **89**, 607 (1996).

[29] I. S. McDermid, J. Chem. Soc. Faraday Trans. II **77**, 519 (1981).

[30] W. A. de Jong, J. Styszynski, L. Visscher, and W. C. Nieuwpoort, J. Chem. Phys. **108**, 5177 (1970).

[31] R. D. Amos, A. Bernhardsson, A. Berning *et al.*, MOLPRO, a package of *ab initio* programs designed by H.-J. Werner and P. J. Knowles, version 2008.3.

[32] J. M. Carr, P. G. Galiatsatos, J. D. Gorfinkiel, A. G. Harvey, M. A. Lysaght, D. Madden, Z. Mašín, M. Plummer, J. Tennyson, and H. N. Varambhia, Eur. Phys. J. D **66**, 58 (2012).

[33] J. Tennyson, D. B. Brown, J. J. Munro, I. Rozum, H. N. Varambhia, and N. Vinci, J. Phys.: Conf. Ser. **86**, 012001 (2007).

[34] J. Tennyson, Phys. Rep. **491**, 29 (2010).

[35] A. U. Hazi, Phys. Rev. A **19**, 920 (1979).

[36] W. Domcke, Phys. Rep. **208**, 97 (1991).

[37] D. J. Haxton, C. W. McCurdy, and T. N. Rescigno, Phys. Rev. A **73**, 062724 (2006).

[38] D. T. Birtwistle and A. Herzenberg, J. Phys. B **4**, 53 (1971).

[39] R. J. Hall, J. Chem. Phys. **68**, 1803 (1978).

[40] J. N. Bardsley and J. M. Wadehra, J. Chem. Phys. **78**, 7227 (1983).

[41] J. N. Bardsley, in *Electron-Molecule and Photon-Molecule Collisions*, edited by T. Rescigno, V. McKoy, and B. Schneider (Plenum, New York, 1979).

[42] I. I. Fabrikant and H. Hotop, Phys. Rev. A **63**, 022706 (2001).

[43] D. R. Lide, in *Handbook of Chemistry and Physics*, 96th ed., edited by W. M. Haynes (CRC Press, Orlando, FL, 2015), p. 51, Sect. 9.

[44] I. I. Fabrikant and H. Hotop, J. Chem. Phys. **128**, 124308 (2008).

[45] T. Su and W. J. Chesnavich, J. Chem. Phys. **76**, 5183 (1982); T. Su, *ibid.* **89**, 5355 (1988); **88**, 4102 (1988). We used the parametrized formula given in the final citation, except that the dimensionless temperature T_R is misprinted; $T_R = 2\alpha k_B T/\mu_D^2$. In evaluating this expression, we used tabulated dipole moments (Ref. [43]) and assumed that the polarizabilities of the interhalogens were the averages of those of the homonuclear halogens, based on tabulated polarizabilities (Ref. [45]).

[46] T. M. Miller, in *Handbook of Chemistry and Physics*, 96th ed., edited by W. M. Haynes (CRC Press, Orlando, FL, 2015), p. 187, Sect. 10.

[47] P. Španěl, M. Tichy, and D. Smith, Int. J. Mass Spectrom. Ion Processes **129**, 155 (1993).